journal of the mechanical behavior of biomedical materials 154 (2024) 106531

Contents lists available at ScienceDirect

Journal of the Mechanical Behavior of Biomedical Materials

journal homepage: www.elsevier.com/locate/jmbbm

Exploiting light-based 3D-printing for the fabrication of mechanically enhanced, patient-specific aortic grafts

Lisa Asciak [a], Roger Domingo-Roca [b], Jamie R. Dow [a,c], Robbie Brodie [c], Niall Paterson [c], Philip E. Riches [a], Wenmiao Shu [a], Christopher McCormick [a,*]

[a] Department of Biomedical Engineering, University of Strathclyde, Glasgow, UK
[b] Department of Electronic and Electric Engineering, University of Strathclyde, Glasgow, UK
[c] Research and Development, Terumo Aortic Ltd., Inchinnan, Glasgow, UK

ARTICLE INFO

Keywords:
Aortic synthetic grafts
Biomechanical mismatch
Alginate:PEGDA interpenetrating polymer network
Stereolithography 3D-printing
Free-standing tubular hydrogels
Personalised vascular grafts

ABSTRACT

Despite polyester vascular grafts being routinely used in life-saving aortic aneurysm surgeries, they are less compliant than the healthy, native human aorta. This mismatch in mechanical behaviour has been associated with disruption of haemodynamics contributing to several long-term cardiovascular complications. Moreover, current fabrication approaches mean that opportunities to personalise grafts to the individual anatomical features are limited. Various modifications to graft design have been investigated to overcome such limitations; yet optimal graft functionality remains to be achieved. This study reports on the development and characterisation of an alternative vascular graft material. An alginate:PEGDA (AL:PE) interpenetrating polymer network (IPN) hydrogel has been produced with uniaxial tensile tests revealing similar strength and stiffness (0.39 ± 0.05 MPa and 1.61 ± 0.19 MPa, respectively) to the human aorta. Moreover, AL:PE tubular conduits of similar geometrical dimensions to segments of the aorta were produced, either via conventional moulding methods or stereolithography (SLA) 3D-printing. While both fabrication methods successfully demonstrated AL:PE hydrogel production, SLA 3D-printing was more easily adaptable to the fabrication of complex structures without the need of specific moulds or further post-processing. Additionally, most 3D-printed AL:PE hydrogel tubular conduits sustained, without failure, compression up to 50% their outer diameter and returned to their original shape upon load removal, thereby exhibiting promising behaviour that could withstand pulsatile pressure *in vivo*. Overall, these results suggest that this AL:PE IPN hydrogel formulation in combination with 3D-printing, has great potential for accelerating progress towards personalised and mechanically-matched aortic grafts.

1. Introduction

Cardiovascular disease (CVD) remains the leading cause of mortality and morbidity worldwide (Roth et al., 2020). CVD manifests itself in different forms, with aneurysm formation within the aorta posing a significant threat to life due to potential rupture, if not diagnosed and treated at early stages. Aortic aneurysms at risk of rupture, indicated by an increase in aneurysm diameter, are treated surgically by means of synthetic, large-diameter vascular grafts (Golledge, 2019; Swerdlow et al., 2019). Most state-of-the-art synthetic aortic grafts are made of woven or knitted polyester (polyethylene terephthalate; PET or Dacron®) fabric and present several advantages, such as off-the-shelf availability, durability, reasonable biocompatibility, ease of suturability, and overall satisfactory post-operative outcomes (Bustos et al., 2016; Spadaccio et al., 2016). Nevertheless, such materials have a range of limitations that hinder their full potential when used as an aortic implant. Dacron®, for example, is unable to mimic the biomechanical behaviour of the native aorta since it is a rigid material with stiffness values ten times higher than that of the human aorta (Tremblay et al., 2009; Faturechi et al., 2019). Hence, such grafts are unable to dilate radially to accommodate pulsatile flow in a similar manner to adjoining aortic tissue (Tai et al., 2000). This mismatch in radial compliance has been associated with the disruption of blood flow, thereby contributing to several cardiovascular complications, including high blood pressure, heart strain, and limited blood supply to major organs (Obrien et al., 2008; Ioannou et al., 2009; Vardoulis et al., 2011; Spadaccio et al., 2016; Lejay et al., 2019). Additionally, the aorta is a highly complex, laminated structure that exhibits unique biomechanical characteristics such

* Corresponding author.
E-mail address: christopher.mccormick@strath.ac.uk (C. McCormick).

https://doi.org/10.1016/j.jmbbm.2024.106531
Received 25 August 2023; Received in revised form 28 March 2024; Accepted 29 March 2024
Available online 30 March 2024

as non-linear stress-strain response, viscoelasticity, and anisotropy (Camasão and Mantovani, 2021), which have yet to be fully translated to synthetic vascular grafts (Singh et al., 2015). Despite the vast catalogue of commercially available vascular prostheses, these grafts do not adequately accommodate the intrinsic aortic geometries that vary from one patient to another, ultimately leading to disruptions arising from structural incompatibilities (Singh et al., 2015; Zia et al., 2022). Recent vascular graft research has largely focussed on the development of small-diameter blood vessels, and few attempts have been made to address the shortcomings associated with larger diameter synthetic conduits. For small-diameter blood vessels, the use of hydrogels has been widely investigated, due to the hydrophilicity and similarity of these materials to the extracellular matrix (ECM) of mammalian tissue (González-Díaz and Varghese, 2016). Furthermore, hydrogels can be fabricated using a variety of methods that allow precise control over a set of chemical, mechanical, and physical properties (Wang et al., 2020). One such method is 3D-printing, which has demonstrated great potential for rapid production of personalised components for biomedical applications in a cost-efficient manner (Melchiorri et al., 2016; Holland et al., 2018).

Various monomers have been investigated towards the fabrication of biocompatible hydrogels for vascular tissue engineering, with alginate being one of the most commonly used materials (Gao et al., 2015; Ghanizadeh Tabriz et al., 2015; Antunes et al., 2021). Its popularity in the biomedical field is largely attributed to its biocompatibility and ease of gelation in the presence of divalent cations (e.g., Ca^{2+}) (Lee and Mooney, 2012; Cattelan et al., 2020). However, as with most naturally derived monomers, single-network, ionically-crosslinked alginate hydrogels exhibit poor mechanical strength when compared with the native vasculature (Liu et al., 2015; Krishnamoorthy et al., 2019). One way to address this issue is the development of interpenetrated polymer networks (IPNs), where two or more monomers are combined, crosslinked separately, and therefore not covalently bound to each other (Chimene et al., 2020). Hence, the final hydrogel, in most cases, benefits from the favourable properties of each of the individual components (Parak et al., 2019), resulting in improved stiffness, strength, and fracture energy whilst maintaining extensibility (Sun et al., 2012; Hong et al., 2015). An example of this approach is the use of an ionic-covalent entanglement (ICE), which combines ionically- and covalently-crosslinked polymers (Sun et al., 2012; Hong et al., 2015). The most used covalently-crosslinkable polymer is polyethylene glycol diacrylate (PEGDA), since it is reported to be biologically inert with low thrombogenicity, thereby making it an attractive material for use within artificial blood vessels (Munoz-Pinto et al., 2015). Additionally, due to its photosensitivity in the presence of a photoinitiator, PEGDA is suitable for light-based 3D-printing – a printing modality that exploits light-responsive resins to produce solid parts in a layer-by-layer fashion upon exposure to ultraviolet (UV) or visible light. Despite the combination of ionically crosslinked alginate and covalently crosslinked PEGDA having been already reported (Hong et al., 2015), this material combination has yet to be exploited in light-based 3D-printing. Moreover, despite the recent emergence of light-assisted 3D-printing of hydrogels for biomedical applications (Yu et al., 2020; Murphy et al., 2022; Levato et al., 2023; Asciak et al., 2023), this 3D-printing method remains to be implemented for the fabrication of large-diameter tubular structures for aortic graft applications. Potentially, this is due to the persistent challenge associated with most 3D-printing platforms when producing high aspect ratio structures in the vertical direction involving the eventual collapse of these long structures as a result of gravitational forces (Tan and Yeong, 2015; Khilnani et al., 2023). Apart from controlling 3D-printing parameters, such as first layer exposure time in stereolithography 3D-printing to ensure proper adhesion to the platform, preventing structure collapse also highly depends on the resin (hydrogel formulation) as this must be robust enough to withstand the weight of the printed structure (Tan and Yeong, 2015). Therefore, given the multiple advantages of both alginate and PEGDA, it is hypothesized that their combination as an ICE IPN will produce a material with superior mechanical characteristics than those currently used as aortic implants, which would also benefit the 3D-printing process, thereby potentially fabricating free-standing tubular structures that can be personalised and are more patient-specific than the current state-of-the-art aortic grafts.

This work addresses the limitations associated with existing aortic grafts by identifying an optimal ionically-crosslinked alginate and PEGDA (AL:PE) IPN hydrogel formulation for the rapid and personalised production of aortic implants via vat photopolymerisation 3D-printing. The results have been compared with those obtained using a conventional moulding approach. Special attention has been paid to the mechanical behaviour, microstructure, and fabrication characteristics of the studied hydrogels since such properties will ultimately dictate the hydrogel's suitability as a replacement for current commercially available aortic grafts. It is further demonstrated that the ICE IPN hydrogel can be used in combination with 3D-printing to rapidly produce long, complex, hollowed structures, that faithfully replicate anatomical structures.

2. Materials and methods

2.1. Materials

Alginic acid sodium salt (M/G ratio of 1.56, viscosity: 15–25 cP 1% in H_2O, molecular weight 120–190 kDa), polyethylene glycol diacrylate (PEGDA) Mn 700, agarose (Type I-A, low EEO), calcium carbonate ($CaCO_3$), glucono-delta-lactone (GDL), barium chloride ($BaCl_2$), calcium chloride ($CaCl_2$), 2-hydroxy-4′-(2-hydroxyethoxy)-2-methylpropiophenone (Irgacure 2959, I2959), lithium phenyl-2,4,6-trimethylbenzoylphosphinate (LAP), tartrazine, and phosphate buffered saline (PBS) tablets, were all purchased from Sigma Aldrich, UK, and used without further modification unless otherwise stated.

2.2. Hydrogel preparation

2.2.1. Casting method

Single-network alginate and AL:PE IPN hydrogels were evaluated as described in Table 1. First, stock solutions of alginate (5% (w/v) or 8% (w/v)) and PEGDA (67% (w/v)) were prepared in deionised (DI) water. For single-network alginate hydrogels, $CaCO_3$:GDL (1:2 M ratio) was identified as the most suitable crosslinking agent (Supplementary Information, (SI) Fig. S1). These hydrogels were prepared by mixing the alginate stock solution (5% (w/v)) with the $CaCO_3$:GDL solution (prepared in DI water) at a 2:1 vol ratio. The alginate:crosslinker solution was then poured into moulds and allowed to set at 4 °C overnight. For

Table 1
Hydrogel formulations, notations, and final concentrations. (PI: photoinitiator, PB: photoblocker, 3DP: 3D-printed).

Hydrogel Formulation	Hydrogel Notation	Alginate (% w/v)	PEGDA (%w/v)	PI (% w/v)	PB (% w/v)	Crosslinker (mM)
Alginate: $CaCO_3$: GDL	AL:CG	3.3	–	–	–	67:133
Alginate: PEGDA: $CaCO_3$: GDL	AL:PE:CG	3.3	27	0.5	–	67:133
Alginate: PEGDA: $BaCl_2$	AL:PE:B	3.3	27	0.5	–	67
Alginate: PEGDA: $BaCl_2$: 3DP	AL: PE:3DP	3.3	27	0.5	0.03	67

the AL:PE IPN hydrogels, the alginate (8% (w/v)) and PEGDA (67% (w/v)) stock solutions were mixed at a 1:1 vol ratio followed by the addition of the photoinitiator to reach the final concentrations presented in Table 1. The solution was stirred at room temperature, followed by degassing cycles in an ultrasonic bath. In the case of $BaCl_2$ crosslinking, the AL:PE IPN solution was first poured into the desired moulds and exposed to UV light (365 nm; 2.2 mW/cm^2 at 10 mm distance) for 30 min for the PEGDA to gel. After gelation, the sample was transferred into a $BaCl_2$ bath for the alginate to crosslink (Fig. 1). For the $CaCO_3$:GDL crosslinker, this was mixed with the AL:PE IPN solution prior to exposure to UV light.

Moulded tubular structures were fabricated using an agarose sacrificial cylindrical structure, the process described schematically in Fig. 2. Briefly, a 2.5% (w/v) agarose solution was prepared by dissolving agarose powder in heated DI water (80 °C). Once fully dissolved, the agarose solution was poured into polypropylene syringes (ID ~12 mm) and left to cool at room temperature. The solidified agarose cylinders were then removed from the syringes and placed into larger polypropylene syringes (ID ~14.5 mm). The AL:PE IPN solution was then poured filling in the gap between the agarose hydrogel and the syringe wall. The syringe containing both the agarose cylindrical gel and the AL:PE IPN solution were then exposed to UV light (365 nm; 2.2 mW/cm^2 at 10 mm distance) for 15 min. Upon PEGDA crosslinking, the whole structure was removed from the syringe and immersed in $BaCl_2$. Following AL:PE IPN hydrogel formation, the structure was placed in a heated DI water bath for the agarose to shrink, leaving behind an AL:PE IPN tubular structure.

2.2.2. Stereolithography (SLA) printing

A commercial desktop 3D printer (PRUSA SL1S, PRUSA Research, Prague, CR) equipped with a 405 nm UV LED panel (Fig. 2B) was used to 3D print discs and dog-bone shaped samples for material mechanical characterisation, and aortic-mimicking tubular structures. The AL:PE IPN resin for 3D-printing was prepared using 0.5% (w/v) LAP as the photoinitiator. To improve 3D-printing resolution, tartrazine was incorporated within the pre-gel mixture to act as a photoblocker given its high absorption at 405 nm (Yang et al., 2020). Different photoblocker concentrations (0%, 0.01%, 0.025%, and 0.03% (w/v)) were investigated to determine optimal 3D-printing resolution. The 3D-printing exposure times were determined by performing cure depth measurements as a function of layer thickness and fitting the results to the Beer-Lambert law (Seo et al., 2017; Benjamin et al., 2019; Domingo-Roca et al., 2022) (SI Fig. S9).

Prior to 3D-printing, the designed target models were prepared via a computer-aided design (CAD) software Autodesk Inventor (Autodesk, Inc.) and exported as STL files. These were then imported into PRUSA Slicer, sliced at 50 μm layer thickness, and exported to the 3D printer for production. Tubular structures of different dimensions: internal diameters (9 mm and 14 mm), wall thicknesses (0.5 mm, 1 mm, and 2 mm), and lengths (7.5 mm and 15 mm), were 3D-printed. The structures were then immersed in a $BaCl_2$ bath for alginate crosslinking. Moreover, to demonstrate the capability of 3D-printing as a fabrication method for faithful replications of aortic geometries, a human abdominal aortic open-source model (*The Biomedical 3D printing community, Embodi3D*, 2023) was used to 3D-print small segments of the aortic tree, including the renal and bifurcation areas.

2.3. Physical characterisation

2.3.1. Morphological analyses

The morphology of all the hydrogel formulations was analysed via scanning electron microscopy (SEM, Hitachi TM 1000). Prior to imaging, hydrogel discs were first frozen at −20 °C for 24 h followed by freeze-drying at −80 °C for another 24 h using a benchtop freeze dryer (Labconco FreeZone®). SEM imaging was carried out on the freeze-dried gels at the surface and at specimen cross-sections.

2.3.2. Water uptake and degradation

Water uptake was analysed in moulded hydrogel discs after freeze-drying. The dry weights were measured (W_{Dry}), followed by immersion of the dried hydrogels in calcium-supplemented PBS (Ca-PBS; 1 × PBS + 1.8 mM $CaCl_2$) and incubated at 37 °C. The hydrogels were weighed following incubation for 2h, 72h, 1 week, 2 weeks, and 3 weeks to obtain wet weights (W_{Wet}). The water uptake ratio was calculated using Equation (1).

$$Water\ uptake = (W_{Wet} - W_{Dry})/W_{Dry} \quad (1)$$

For the degradation analysis, moulded hydrogel discs were freeze-dried at −80°C and the dry weights measured (D_o). The dried hydrogels were immersed in Ca-PBS and incubated at 37 °C. At different timepoints (24 h, 72 h, and 1 week) the gels were freeze-dried again and weighed to obtain dry weights (D_t). The degree of degradation expressed in percentage weight loss was calculated using Equation (2).

$$Weight\ loss\ (\%) = [(D_o - D_t)/D_o] \times 100 \quad (2)$$

2.4. Mechanical characterisation

All mechanical characterisation tests were performed on as-prepared, hydrated hydrogels at room temperature.

2.4.1. Confined compression stress relaxation tests

Confined compression tests were performed on an Electroforce® 3100 test instrument (TA Instruments, Waters Ltd., UK) equipped with a 22 N load cell. Moulded hydrogel discs were tested in 24-well tissue culture plates confining the hydrogels at the sides and base. A stainless-steel flat, porous indenter ($k = 6 \times 10^{-7}$ m^4/N s, 15.6 mm diameter) was used as the compressive plate. The indenter was lowered to touch the hydrogel surface to ensure full contact (applying a preload of 0.1 N), and the system was left to equilibrate prior to running the experiment (approximately 2 h). The confined compression protocol comprised a ramp-hold test to assess the stress-relaxation properties of the gel, obtaining values for compressive peak stress, aggregate modulus (H_A), and hydraulic permeability (k). Following the protocol by Busby et al. (2013), specimens were compressed to 5% of their original thickness at a ramp rate of 0.5%/s, and held at that strain for 300 s. The compressive peak stress was obtained directly from the stress relaxation curve since this corresponds to the maximum stress at the end of the ramp stage. For

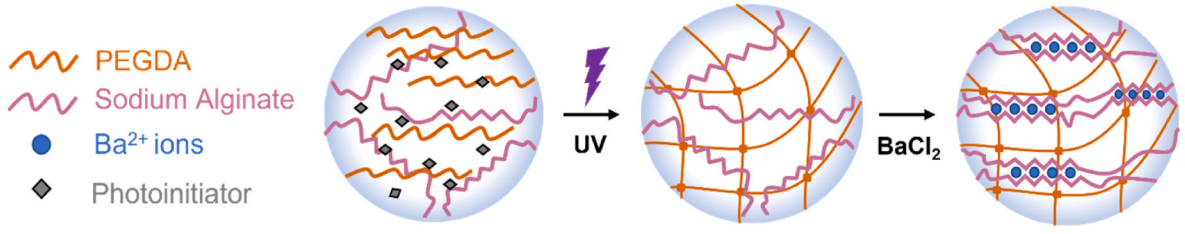

Fig. 1. Schematic representation of the AL:PE IPN hydrogel synthesis process comprising of two crosslinking steps: UV photopolymerisation of the PEGDA followed by ionic crosslinking of the alginate via $BaCl_2$.

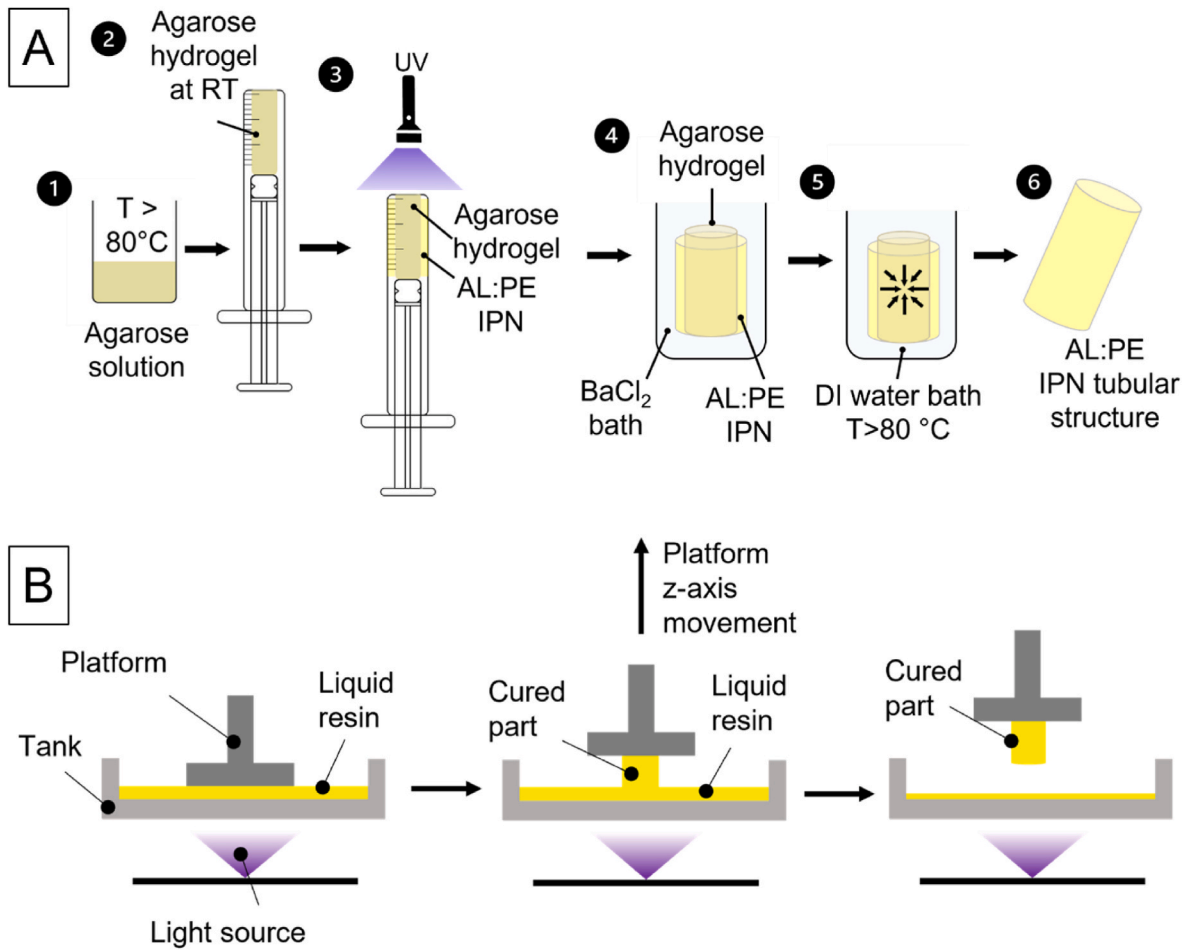

Fig. 2. Schematic representation of (A) the fabrication process of the moulded tubular structures using an agarose sacrificial scaffold, and (B) the mechanism for stereolithography (SLA) 3D-printing.

H_A and k, an open-source finite element analysis software (FEBio 2.9.1) was used to develop a linear biphasic poroviscoelastic (BPVE) model representing the hydrogel in confined compression (SI Fig. S2). The solid phase of the gel was characterised by a compressible, isotropic, visco-elastic neo-Hookean material, the stress relaxation of which was controlled by a single exponential term, with the flow of the fluid through the solid governed by a constant permeability value, (k). Through this model, the experimental stress relaxation curve was iteratively used in a parameter optimisation process to determine the best fit curve thereby eliciting values for H_A and k (SI Fig. S2). By using a Poisson's ratio of zero, given that in confined compression the lateral stresses are negligible, under small strains the derived Young's modulus was equal to the aggregate modulus. All tests were performed in triplicates and at room temperature.

2.4.2. *Uniaxial tensile tests*

Tensile tests were performed using an Instron Electropuls™ (E10000 Linear-Torsion All-Electric Dynamic Test Instrument, UK) equipped with a 1 kN load cell. Moulded and 3D-printed dog-bone shaped (ASTM Type IV) hydrogel specimens were subjected to stretch to failure tests at a crosshead speed of 1 mm/min to assess the ultimate tensile strength (UTS), elastic modulus (E), and elongation at break. Specimen rupture beyond the gauge area was considered as a null test. Tests were performed in air at room temperature with 5 samples for each hydrogel formulation.

2.4.3. *Rheological analysis*

Rheological measurements on moulded and 3D-printed hydrogel disc samples (20 mm diameter, 2 mm thickness) were performed using a rotational rheometer (Netzsch Kinexus Pro+, Germany) fitted with parallel plate geometry (20 mm indenter diameter). To ensure contact between the indenter and the sample, a normal force of 1 N was employed. In order to determine the linear viscoelastic region (LVER) – the region where stress and strain are independent of each other – amplitude sweeps (n = 3) were first performed at shear stresses ranging from 0.01 Pa to 500 Pa at a fixed frequency of 1 Hz. From these tests, a shear strain within the LVER (0.01%) was then selected to perform oscillatory frequency sweeps (n = 5) at a frequency range from 0.1 Hz to 10 Hz. All tests were performed in replicates at room temperature.

2.4.4. *Tubular structure characterisation*

Tubular structures of different internal diameters and wall thicknesses were fabricated both via casting and 3D-printing. The structures were analysed visually, and mechanically characterised by uniaxial compression tests. For the latter, the 3D-printed samples were placed horizontally between two flat plates and compressed to a 50% displacement with respect to their original outer diameter using the Instron Electropuls™ (E10000 Linear-Torsion All-Electric Dynamic Test Instrument, UK).

2.5. *Statistical analysis*

Experimental results are presented as the mean ± one standard deviation (s.d.). All graphs were generated using OriginPro 2020 software and statistical analyses were performed via Minitab 20.0 statistical software. The mechanical properties of different hydrogel formulations

were compared using one-way ANOVA followed by Tukey's *post-hoc* analysis, unless otherwise specified. A $p\text{-value} < 0.05$ was considered statistically significant.

3. Results

3.1. Mechanical characterisation

Confined compression tests on single-network, $CaCO_3$:GDL-crosslinked alginate, and $CaCO_3$:GDL- or $BaCl_2$-crosslinked AL:PE IPN revealed that all hydrogel formulations exhibited a classic stress relaxation response (Fig. 3A). This is characterised by well-defined ramp, peak, and hold phases. As expected, the single-network alginate hydrogel exhibited significantly lower peak stress (1.33 ± 0.10 kPa) when compared to the AL:PE IPN hydrogels (16.67 ± 6.56 kPa and 9.65 ± 2.15 kPa for AL:PE:CG and AL:PE:B, respectively). An almost 6-times increase in H_A was observed between single-network alginate and the IPN hydrogels (Fig. 3B). Conversely, k decreased upon IPN formation (Fig. 3C). When comparing both IPN hydrogel samples, no significant differences in H_A were observed between the $CaCO_3$:GDL and $BaCl_2$ crosslinkers (Fig. 3B).

Uniaxial tensile stretch to failure tests showed a significant increase in both ultimate tensile strength (UTS) (Fig. 3E) and elastic modulus (Fig. 3F) upon IPN formation, however at the expense of elongation at break (Fig. 3D). The choice of the alginate crosslinking agent was observed to play a significant role in the elastic properties of the AL:PE IPN hydrogels, with $BaCl_2$ crosslinking producing double the UTS and elongation at break than the $CaCO_3$:GDL crosslinked IPN. From these results $BaCl_2$ was taken forward as the most suitable crosslinking agent for further mechanical analyses and 3D-printing of AL:PE IPN hydrogels. Interestingly, the latter resulted in no significant differences in elastic properties when compared with the moulded AL:PE IPN hydrogels. However, during the 3D-printing optimisation process, the addition of a photoblocker, tartrazine, to improve 3D-printing accuracy was found to influence the mechanical properties (SI Fig. S10). Following this analysis, the photoblocker concentration that resulted in optimal 3D-printing resolution i.e., the closest geometry to the CAD model (SI Table 6), whilst maintaining the desired mechanical properties, was identified to be 0.03% (w/v).

The viscoelastic properties of AL:CG, AL:PE:B (moulded), and AL:PE:3DP revealed that for AL:PE IPN hydrogels the LVER extends beyond 100 Pa (Fig. 3G) whereas for the single-network alginate a decrease in storage modulus (G') and an increase in loss modulus (G'') was observed (intersecting at a shear stress of 70 Pa). In both amplitude and frequency sweeps (Fig. 3H), G' is much larger than G'', indicating the predominance of the elastic component in all the investigated samples. The 3D-printed hydrogels exhibited the highest G', followed by the moulded IPN hydrogel and the single-network alginate. A slight increase in G' was observed with increasing frequencies, albeit not significant.

3.2. Physical characterisation

3.2.1. Stability of the hydrogels in physiological environments

Fluid uptake and degradation were studied to evaluate the hydrogels' behaviour in physiologically-relevant conditions. Fig. 4A shows that upon IPN formation, the hydrogel's water uptake is significantly less than in the single-network alginate. The latter exhibits a sudden increase in liquid uptake after the first 2 h and continues to swell throughout the rest of the incubation period. In contrast, AL:PE:B reaches an equilibrium state within 2 h of incubation. Similarly, Fig. 4B reveals that AL:CG exhibits greater weight loss than AL:PE:B, especially during the first 72 h of incubation.

3.2.2. Morphological analysis

Examination of the hydrogel's microstructure via SEM imaging provides insight into the role of the hydrogel's porosity in liquid uptake kinetics and its degradation behaviour. Single-network alginate exhibited a high degree of porosity accompanied by a large pore size both at the surface (Fig. 5A) and cross-section (Fig. 5B). The formation of an IPN and high PEGDA monomer concentrations (27% (w/v)) used in this study resulted in a densely crosslinked hydrogel with smaller pores, which are barely visible on the surface of AL:PE:B and AL:PE:3DP surface (Fig. 5C–E) while small diameter pores can be observed in the cross-sectional images (Fig. 5D–F). For the 3D-printed hydrogels, the freeze-drying process resulted in a slight separation of the 3D-printed layers, which can be observed in Fig. 5F.

3.3. Fabrication and characterisation of anatomically relevant tubular structures for aortic graft applications

Tubular structures (18 mm outer diameter; 2 mm wall thickness) were fabricated using an agarose sacrificial mould method (Fig. 6A), and SLA 3D-printing (Fig. 6B) with close accuracy to the CAD model (SI Table 6). Given that the moulding technique relied on the use of polypropylene syringes (as described in Fig. 2A), the range of tubular dimensions fabricated was limited. In contrast, by exploiting 3D-printing, conduit design could be controlled via the CAD software, and in fact, tubular structures of various wall thicknesses and inner diameters were successfully fabricated (SI Fig. S11 and Fig. S12) in a cost- and time-efficient manner. To evaluate radial load capacity, the 3D-printed conduits (outer diameter: 18.34 ± 0.01 mm, wall thickness: 2.08 ± 0.02 mm) were compressed to approximately 50% of their original outer diameter. Different stages of the compression process of the 3D-printed vessels are shown in Fig. 6C. Two out of three 3D-printed tubular samples exhibited signs of shape recovery upon load removal, and one sample failed at a diameter reduction ratio of 0.446 (Fig. 6D).

Following successful identification of the hydrogel formulation providing elastic properties within the range of aortic tissue, its ability to replicate human aortic anatomy was demonstrated. To do so, small sections of the abdominal aorta including the branching into the renal arteries (Fig. 7B–E) and the bifurcation into the iliac arteries (Fig. 7F–I) were 3D-printed. Fig. 7 shows that the 3D-printed structures provide precise replicas of these anatomical regions.

4. Discussion

Vascular graft-related complications, stemming from discrepancies in the elastomechanical properties and structural incompatibilities to the native aorta, remain a persistent challenge in vascular surgery and have yet to be properly addressed. Therefore, the aim of this work was to develop synthetic, large-diameter tubular conduits as potential replacement for existing aortic Dacron® grafts. The conduits were designed to mimic: (1) the biomechanical behaviour, and (2) anatomical geometry of the native human aorta. To achieve this, a hydrogel-based graft material which is also compatible with light-based 3D-printing was explored, since this method has demonstrated promising results for the production of micron-sized, artificial vascular networks (Grigoryan et al., 2019; Domingo-Roca et al., 2022; Ma et al., 2022), but has yet to be explored for larger diameter blood vessels, such as the aorta.

Sodium alginate was selected as one of the primary monomers of the hydrogel given its ease of gel-forming ability, biocompatibility, and structural similarities to the ECM (Lee and Mooney, 2012), that render it suitable for vascular tissue engineering applications (Ghanizadeh Tabriz et al., 2015, 2017; Antunes et al., 2021). However, as shown in Fig. 3, single-network, ionically crosslinked alginate hydrogels (AL:CG) exhibit weaker mechanical properties when compared to native tissue, limiting their use in load-bearing applications (Ji et al., 2022). This may be attributed to the high-water content of such hydrogels (approximately 97% for the AL:CG) and their large porous microstructure (Fig. 5A and B) that contribute to low strength and stiffness values (23.98 ± 7.85 kPa, and 41.94 ± 5.20 kPa, respectively (Fig. 3E and F)). To enhance the mechanical properties of alginate hydrogels, an ICE IPN was developed

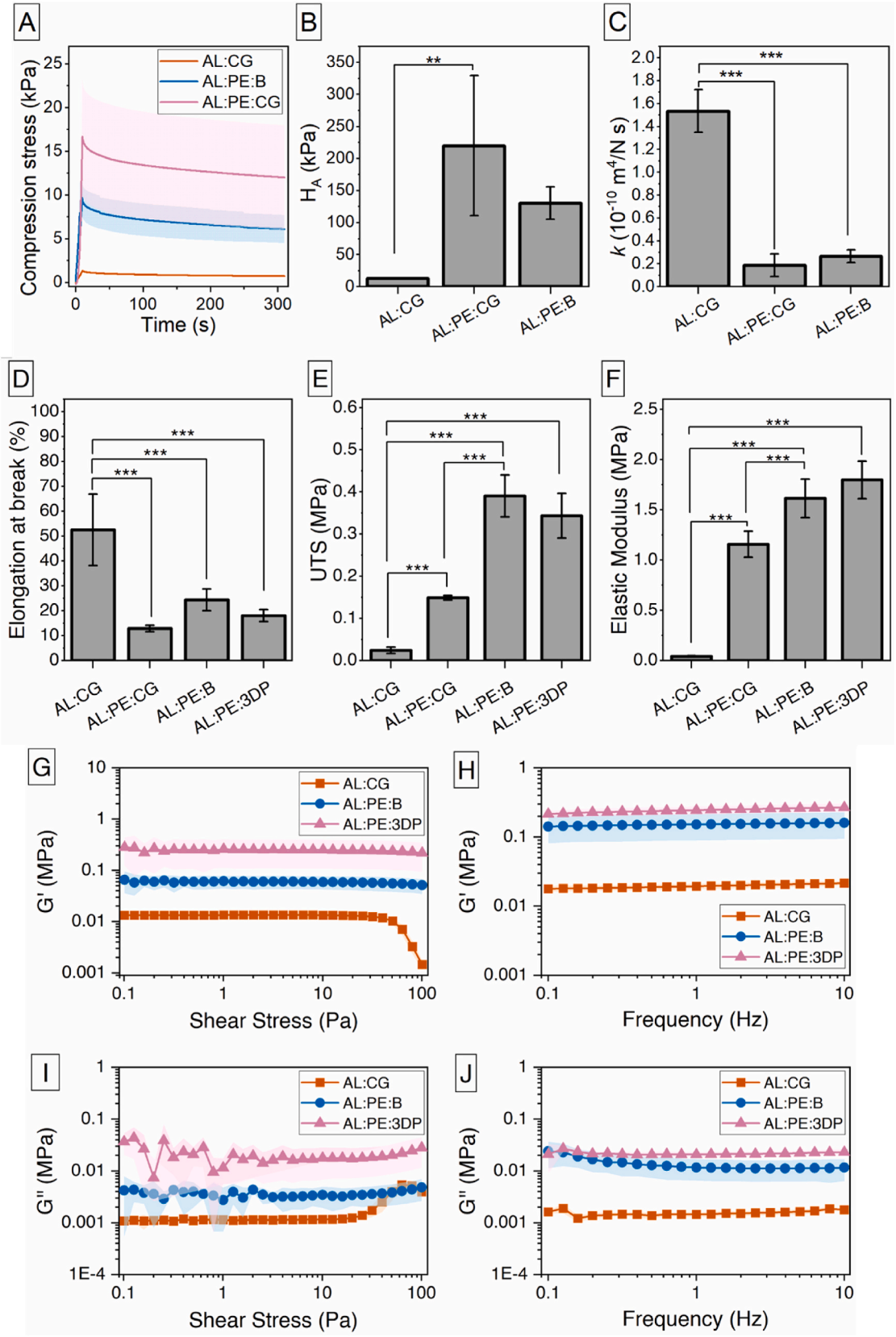

Fig. 3. Mechanical behaviour of single network ionically crosslinked alginate (AL:CG), and alginate:PEGDA IPN (moulded (AL:PE:B) and 3D-printed (AL:PE:3DP)). (A) Confined compression experimental mean stress relaxation curves, (B) aggregate modulus (H_A), and (C) hydraulic permeability (k) properties derived from the biphasic poroviscoelastic model (n = 3 ± s.d.). (D) Elongation at break, (E) ultimate tensile strength (UTS), and (F) elastic modulus from uniaxial tensile stretch to failure tests (n = 5 ± s.d.). (G) Storage modulus (G′) versus shear stress, and (H) storage modulus versus frequency, (I) loss modulus (G″) versus shear stress, and (J) loss modulus versus frequency, from amplitude and frequency sweeps rheological measurements (axes are in logarithmic scale). Statistical significance was measured via one-way ANOVA with Tukey post-hoc analysis and represented graphically by *p < 0.05, **p < 0.01, and ***p < 0.001.

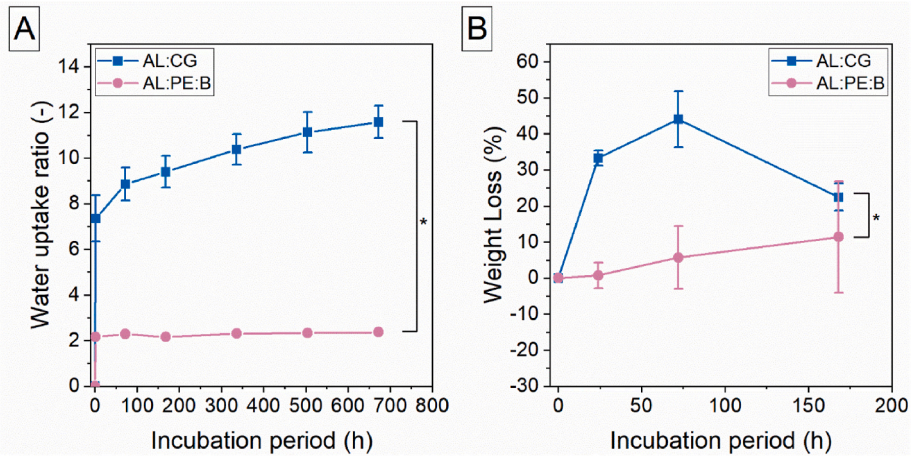

Fig. 4. (A) Water uptake, and (B) degradation analysis in calcium-supplemented PBS (Ca-PBS) at 37 °C over a period of 3 weeks and 1 week, respectively (n = 6 ± s.d.) for single-network alginate (AL:CG) and moulded alginate:PEGDA IPN (AL:PE:B). Significance was assessed via 2-sample independent *t*-test and represented graphically by *p < 0.05.

by introducing PEGDA to the alginate. The advantages of developing IPN hydrogels have been documented in several investigations (Sun et al., 2012; Xu et al., 2019; Chimene et al., 2020), including the combination of alginate:PEGDA IPN hydrogels (Hong et al., 2015; Cristovão et al., 2019; Zhang et al., 2021). Such studies have mostly relied on conventional calcium-based crosslinkers ($CaCl_2$ or $CaSO_4$) to induce alginate gelation, high molecular weight (MW) PEGDA (greater than 1000 Da), and fabrication methods involving either casting or extrusion-based 3D-printing. In this study, an alternative AL:PE IPN hydrogel fabrication strategy is proposed by introducing a barium-based alginate crosslinker ($BaCl_2$), a lower molecular weight PEGDA (700 Da), whilst exploiting an inexpensive, commercially-available SLA 3D printer.

An IPN comprising alginate and PEGDA has been demonstrated to achieve mechanically tough yet highly stretchable hydrogels owing to: (1) the covalent crosslinking of PEGDA, which allows for a high degree of elasticity even under large deformations, and (2) the ionic crosslinking of the alginate via divalent cations, which provides energy dissipation during the breaking and reforming of the physical crosslinks (Sun et al., 2012; Hong et al., 2015). The results reported here via stretch to failure tensile tests, demonstrated a significant increase in strength and stiffness of IPNs when compared with single-network alginate hydrogels (Fig. 3E and F), however at the expense of elongation at break (between 20% and 30% as opposed to 50% of AL:CG (Fig. 3D)). The elasticity of PEGDA is highly dependent on its molecular weight (MW) and weight concentration, but also on other factors such as photoinitiator concentration, UV or light exposure time and intensity. Studies have reported that the higher the MW of PEGDA, the longer the monomer chain, and therefore the lower the crosslinking density, resulting in less stiff (lower elastic modulus) and more extensible hydrogels (Zhang et al., 2011; Hong et al., 2015). Therefore, the elongation of the AL:PE IPN hydrogel reported in the present work (24.4 ± 4.33% and 18.02 ± 2.41% for the moulded and 3D-printed, respectively) is to be expected considering the high concentration of PEGDA within the IPN (27% w/v) and its MW (700 Da). Similar studies have reported elongation values over 100% for PEGDA MWs ranging from 6000 to 20000 Da (Hong et al., 2015; Zhang et al., 2021). In addition to the work presented here, the effect of different PEGDA molecular weights (Mn 575 and Mn 10000) on the AL:PE IPN hydrogel was also investigated (SI Fig. S4-S6). By introducing a small amount of high MW PEGDA (Mn 10000), an increase in extensibility was observed, yet both strength and stiffness exhibited a decrease (SI Fig. S6), and therefore this hydrogel formulation was not taken forward for further investigation. Despite the elongation obtained in this work not being comparable with that reported in other AL:PE IPN studies, herein the moulded IPN comprising PEGDA with a MW of 700 Da and a concentration of 27% (w/v) resulted in extensibility close to that reported in the literature for the aorta (AL:PE:B: 24.4 ± 4.33% versus 29.0 ± 4.0% for the human abdominal aorta (Vallabhaneni et al., 2004)).

Furthermore, in this study a barium-based alginate crosslinker was investigated instead of the conventional and widely explored calcium crosslinkers (Kuo and Ma, 2001; Growney Kalaf et al., 2016). The use of barium-based crosslinkers has been shown to improve both the mechanical properties, and the stability of calcium crosslinked alginate hydrogels in physiological conditions when used as a secondary crosslinker (Ghanizadeh Tabriz et al., 2015; Antunes et al., 2021). This happens because Ba^{2+} ions have a greater affinity to alginate and a larger ionic radius than Ca^{2+} ions, which form tighter crosslinks and, thus, stronger ionic bonds (Mørch et al., 2006; Jejurikar et al., 2011). Here, this hypothesis is evident in the tensile test results (Fig. 3D–F), where AL:PE:B resulted in the highest strength and stiffness values (0.39 ± 0.05 MPa and 1.61 ± 0.19 MPa, respectively), almost double than AL:PE:CG. When investigating the mechanical properties of single-network alginate, it was difficult to obtain uniformly crosslinked, well-defined samples via $BaCl_2$ owing to its instantaneous gelling mechanism (SI Fig. S1). Therefore, since hydrogel shape uniformity is essential for accurate material characterisation measurements, single-network alginate hydrogels were fabricated using an internal, slow gelling calcium-based crosslinker ($CaCO_3$:GDL). In this case, alginate hydrogel uniformity is obtained due to the low solubility of $CaCO_3$ in water which requires the addition of GDL as a catalyst to activate the release of calcium ions in a controlled manner (Kuo and Ma, 2001, 2008).

A limitation associated with the use of ionically crosslinked alginate hydrogels is poor long-term stability due to the exchange of divalent cations with sodium ions present in the surrounding physiological media (Lee and Mooney, 2012; Krishnamoorthy et al., 2019). In the present study, this could be observed by the degradation behaviour of the AL:CG single-networked hydrogels (Fig. 4B) where an increase in weight loss could be observed during the first 72 h of incubation suggesting ion exchange accompanied by the decrosslinking and dissolution of the alginate matrix (Antunes et al., 2021). Interestingly, this was followed by a decrease in weight loss after 1 week of incubation, which might be attributed to re-crosslinking of the alginate due to the presence of the additional Ca^{2+} ions (1.8 mM $CaCl_2$) in the incubation media, contributing to an overall weight gain of the alginate hydrogel (Kuo and Ma, 2008). The incubation behaviour of the AL:PE:B involving a significantly lower water uptake (Fig. 4A) and weight loss (Fig. 4B) in comparison with the single-networked AL:CG hydrogels is also consistent with the

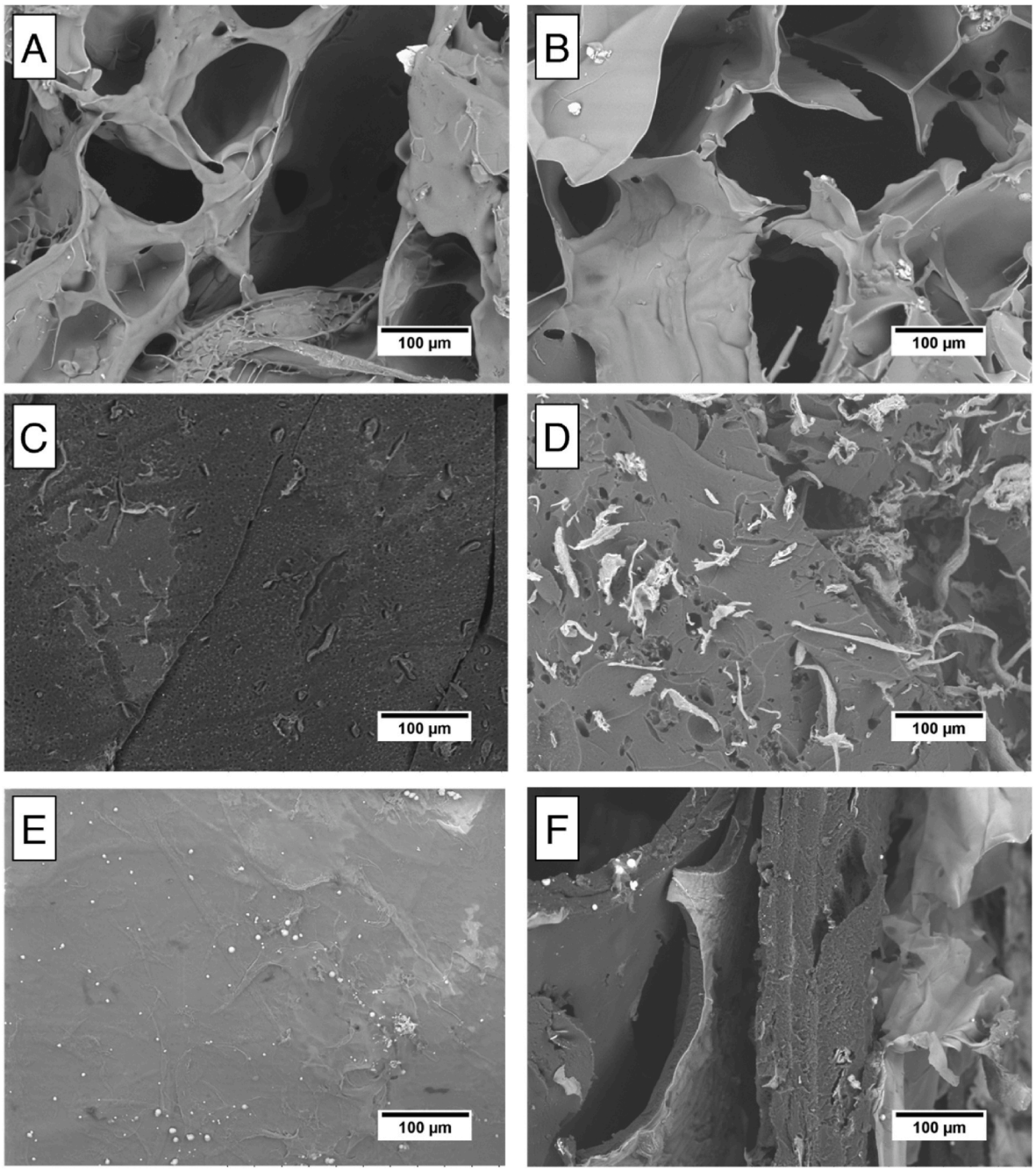

Fig. 5. SEM images of freeze-dried hydrogel samples: surface (A,C,E) and cross-sectional (B,D,F) micrographs of AL:CG (A, B), AL:PE:B (C,D) and AL:PE:3DP (E,F), respectively.

higher monomer content (approximately 30 %(w/v) as opposed to the 3 %(w/v) alginate) and crosslinking density present in the IPN system developed. Therefore, it is hypothesized that the lack of swelling and weight loss exhibited by the IPN hydrogel could potentially contribute to minimal changes in the material's mechanical properties if this were to be implanted *in vivo*. To validate this, a short incubation study was conducted to investigate the mechanical behaviour via uniaxial tensile stretch to failure tests of the AL:CG and AL:PE:B hydrogels following 24 h and 72 h immersion in Ca-PBS at 37 °C (SI Fig. S7). Indeed, the AL:PE:B hydrogels exhibited a decrease in elastic properties when compared to the as-prepared hydrogels (0 h), however this was only significant in the UTS. Given that this evaluation involved timepoints at such early stages in the incubation period, hydrogel swelling was potentially a contributing factor to this weaker strength behaviour. It is important to note that this is a very simplistic and short *in vitro* incubation study, and there are other factors that could affect the long-term mechanical properties of this hydrogel formulation as an aortic graft material, including the difference between the fabrication methods (since the incubation study was performed on moulded samples and not 3D-printed ones), the cellular-biomaterial interaction, hemocompatibility, and blood flow. The precise impact of such factors will require further investigation. The limited water uptake of the IPN hydrogel may also be attributed to the smaller pore size when compared to the single-network alginate as demonstrated by the SEM images in Fig. 5. The increase in crosslinking density upon IPN formation was also evident in the reduction of hydraulic permeability obtained by confined compression stress relaxation FEBio analysis, indicating more resistance to fluid flow (Fig. 3C).

Overall, the AL:PE IPN hydrogel (with PEGDA of Mn 700 Da and

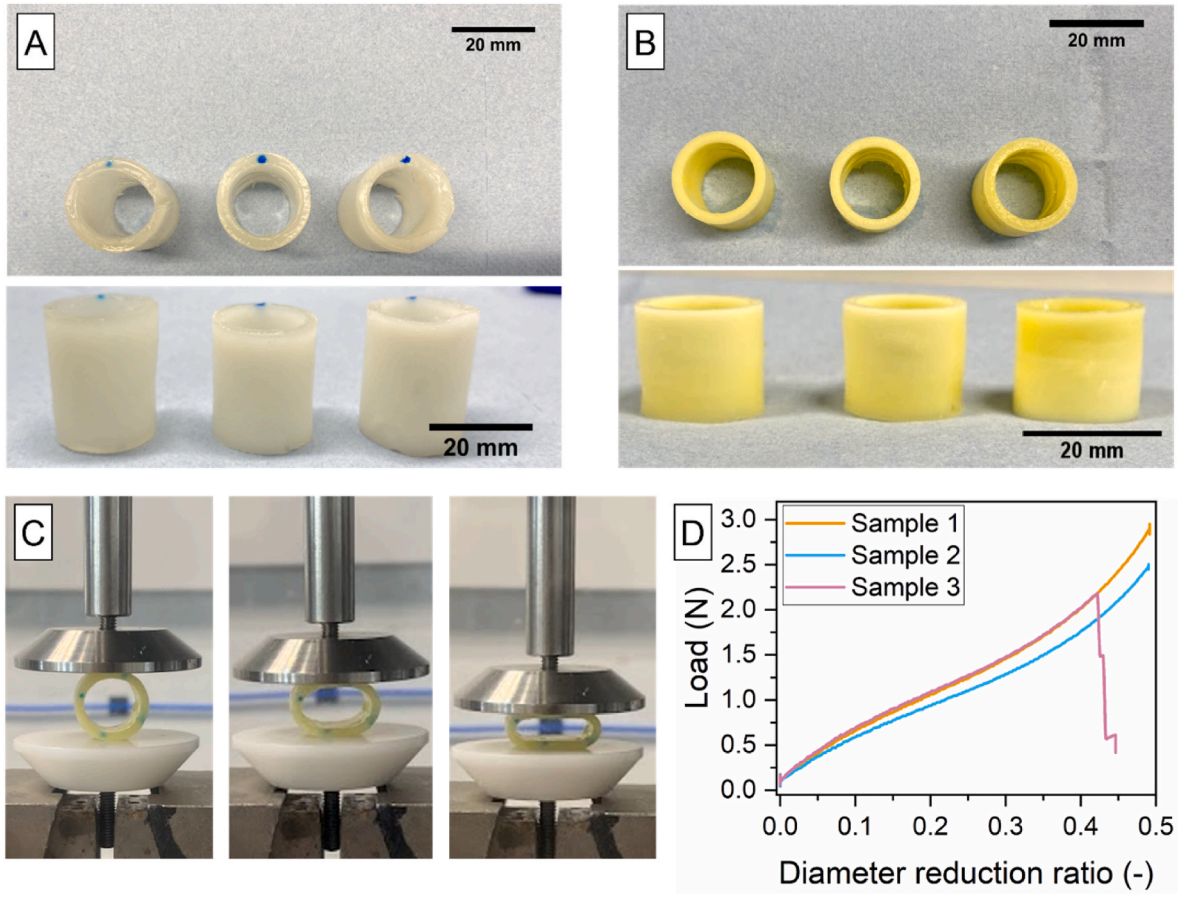

Fig. 6. Tubular structure fabrication via (A) casting using an agarose sacrificial mould, and (B) SLA 3D-printing. (C) Visual representation of 3D-printed tubular vessels during compression to 50% of their original outer diameter. (D) Load versus diameter reduction ratio for the 3D-printed tubular vessels when compressed to 50% of their outer diameter.

$BaCl_2$ as the alginate crosslinker) exhibited the closest elastic mechanical properties (AL:PE:B strength: 0.39 ± 0.05 MPa, stiffness: 1.61 ± 0.19 MPa, and elongation at break: 24.4 ± 4.33%) to the human aorta (elongation at break: 29.0 ± 4.0%, UTS: 0.61 ± 0.07 MPa, elastic modulus: 1.82 ± 0.10 MPa for the human abdominal aorta in the circumferential direction (Vallabhaneni et al., 2004; Teng et al., 2015). These values still show that further optimisation is required especially due to the differences between elongation and strength. Yet, the proposed hydrogel formulation still provides closer elastic properties to the native human aorta than the clinical state-of-the-art Dacron® material, where stiffness values for the latter were measured to be approximately 10 MPa at physiological pressures and 40 MPa at material rupture (SI Fig. S3), consistent with values reported in the literature (Michael Lee and J. Wilson, 1986; Bustos et al., 2016). Overall, matching mechanical data to soft tissue in the literature is complex owing to different variables that affect these measurements, including testing conditions such as crosshead speed or strain rate, temperature, hydration state (dry/wet testing); specimen dimensions, shape (rectangular/dog-bone/tubular), and orientation (longitudinal/circumferential), amongst several other factors. For this reason, the hydrogel specimen gauge length (25 mm) and crosshead speed (1 mm/min) were selected to closely match those use in the aortic tissue investigation of Vallabhaneni et al. (2004). For future investigations, in-house characterisation of aortic tissue using the same testing parameters and conditions would be ideal.

Another key feature in aortic biomechanics is the preservation of the Windkessel effect (i.e., the dampening of pulsatile blood flow as it emerges from the heart's left ventricle to a nearly continuous distal flow) which is fundamental for blood pressure regulation and perfusion to major organs (Huang et al., 2019; Amabili et al., 2020), and this is possible due to the viscoelastic behaviour of the aorta. Hence, an ideal aortic graft must also exhibit similar viscoelastic properties to native aortic tissue. Several characterisation methods have been implemented to assess viscoelasticity of hydrogels, most commonly via stress relaxation tests and rheological assessments. In this work, stress relaxation was carried out in a confined compression set-up. It is important to note that compression tests are not ideal when evaluating the mechanical properties of a material for vascular graft applications given that blood vessels are in a state of tension under physiological loads (Krishnamoorthy et al., 2019; Camasão and Mantovani, 2021). However, the small amount of material required for compression tests was useful in identifying the most promising hydrogel formulations prior to further mechanical analyses. Also, this testing method in combination with the FEBio model enabled the determination of several parameters that cannot be directly elicited from the experimental stress-time curve (i.e., H_A and k). In determining values of H_A and k from the numerical model, these parameters were best-fitted in the muti-dimensional space, alongside other parameters. Whilst the coefficient of determination (R^2) measurements revealed very good fits (SI Table 3 and SI Table 4), there is always the possibility in such scenarios that alternative parameter sets would fit the data equally or better. The typical stress relaxation behaviour was observed in both the single-network alginate and the AL:PE IPN hydrogels (Fig. 3A). Rheological analysis revealed frequency-dependent behaviour of all hydrogel samples (Fig. 3H), a characteristic of healthy arterial tissue (Zhijie et al., 2016). This was observed in the frequency sweep measurements presented in Fig. 3H, with G' increasing with frequency for all three hydrogel samples. It is important to note that typically, storage and loss moduli for aortic tissue are measured using dynamic mechanical analysis (E' and E'',

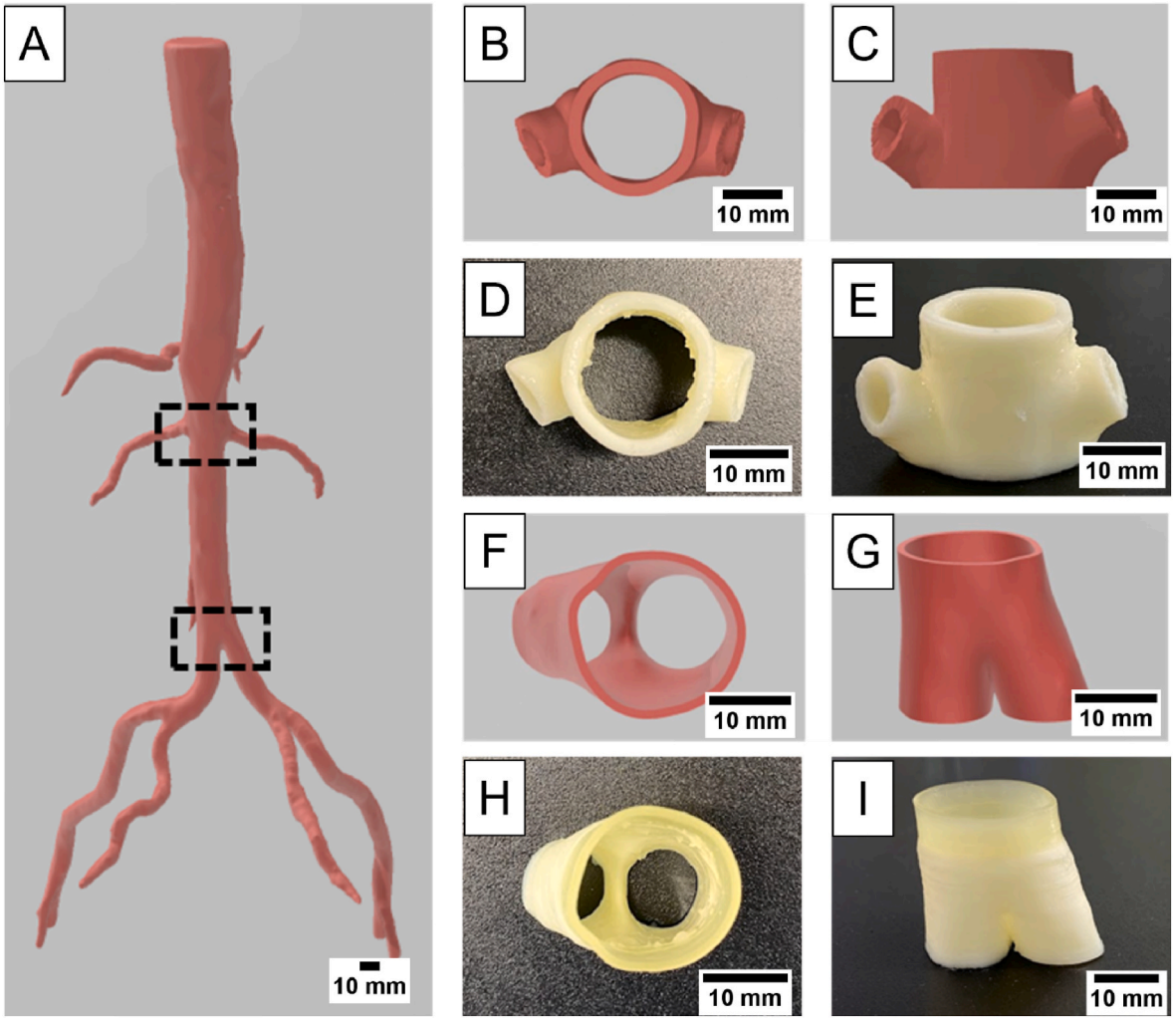

Fig. 7. 3D-printing of an anatomically relevant aortic structure. (A) Open-source human abdominal aorta model (The Biomedical 3D printing community, Embodi3D, 2023) with target model segments marked in dashed boxes. (B) Top and (C) side view of the aortic segment target model that branches into the renal arteries. (D) Top and (E) side view of the 3D-printed branched vessel using AL:PE hydrogel IPN with 0.03% (w/v) photoblocker. (F) Top and (G) side view of the aortic bifurcation target model. (H) and (I) Top side view of the 3D-printed aortic bifurcation using AL:PE hydrogel IPN with 0.03% (w/v) photoblocker.

respectively) where the specimen is subjected to sinusoidal load oscillations in a tensile setup rather than subjected to a shear load. However, shear behaviour of arterial substitutes is still an important parameter given that *in vivo* the lumen experiences shear stresses arising from blood flow. In this work, the amplitude sweeps conducted at shear stresses ranging from 0.01 Pa to 100 Pa showed that the AL:PE IPN hydrogel formulation (both moulded and 3D-printed) are stable up to 100 Pa with no evidence of polymer network breakdown, and thus are able to sustain shear stresses higher than the wall shear stress typically observed in the healthy human aorta (1 Pa and 2.5 Pa in the aortic arch and descending aortic regions (Callaghan and Grieve, 2018)).

In terms of printability, the use of AL:PE IPN as a resin for vat photopolymerisation 3D-printing has not, to the authors' knowledge, yet been reported. In this work, the resin was calibrated and optimised for 3D-printing by varying the photoblocker concentration, which directly controls light penetration depth through the liquid resin and prevents light scattering (Seo et al., 2017; Benjamin et al., 2019; Hisham et al., 2022; Asciak et al., 2023). Hence, an optimised concentration of photoblocker ensures that no overcuring takes place and that there is sufficient bonding between layers, thus maintaining the geometrical and morphological accuracy of the designed target model. In this work, 0.03% (w/v) tartrazine resulted in a significantly lower elongation at break when compared with moulded samples (SI Fig. S10 (A)). However, given that no significant changes in strength (SI Fig. S10 (B)) and stiffness (SI Fig. S10 (C)) were observed, and due to its close geometrical representation to the CAD model (SI Table 5), this was identified as the optimal photoblocker concentration and used in all hydrogel formulations for 3D-printing. Through SLA 3D-printing, self-standing tubular structures with geometries similar to the native human aorta and lengths up to 30 mm were successfully fabricated with printing times ranging between 45 and 60 min (depending on the geometry) without the need for sacrificial cylindrical moulds, followed by crosslinking of the alginate in a bath of $BaCl_2$. Additionally, since SLA does not require the use of an extruder, resin viscosity limitations are minimal which, in turn, enhances the choice of resins that can be used, even if low viscosity resins (<5 Pa s) have been shown to facilitate the 3D-printing process (Mondschein et al., 2017; Ni et al., 2018; González et al., 2020). Hong et al. (2015) investigated the printability of alginate: PEGDA IPNs using an extrusion 3D printer, which required the addition of nanoclay (Laponite) to enhance the viscosity of the pre-gel solution and its shear thinning properties. In this work, this was not necessary, since the viscosity of the resin was less than 1 Pa s (SI Fig. S8), and therefore no additional components (apart from those detailed in Table 1) were added to the resin. Thus, another promising aspect of exploiting this method in tissue engineering is the fact that it allows for the incorporation of biological components within the resin, such as

cells, without the shear stress-induced damages typically associated with nozzle-based printing (Boularaoui et al., 2020).

Moreover, tensile testing showed no significant differences between the stiffness of moulded and 3D-printed AL:PE IPN hydrogels. However, the 3D-printed AL:PE IPN hydrogels exhibited a lower elongation at break (18.02 ± 2.41%) and UTS (0.34 ± 0.05 MPa) when compared with their moulded counterparts (24.4 ± 4.33% and 0.39 ± 0.05 MPa, respectively). This might be attributed to the 3D-printing fabrication process which involves the build-up of the structure in a layer-by-layer fashion which might potentially contribute to structural imperfections (Burke et al., 2020). Additionally, during tensile testing the layered nature of the 3D-printed hydrogel might have contributed to inter-layer shear, acting as a weak point of the structure, thereby facilitating rupture, and weakening the overall strength of the material. Part orientation in SLA 3D-printing has also been found to have a great impact on the mechanical behaviour of the final part (Unkovskiy et al., 2018; Saini et al., 2020; Farkas et al., 2023). In this work, dog-bone samples for tensile testing were printed parallel to the build platform and therefore, when subjected to tensile testing the load was exerted along the layers. Modifications to part orientation, such as printing perpendicularly or at a 45-degree angle to the build platform with supporting structures, would likely result in variations in the AL:PE IPN hydrogel's mechanical behaviour. However, this requires further investigation. Additionally, another factor that might have influenced this decrease in elastic properties, is the higher exposure times used when printing the first few layers of the sample to ensure adhesion to the build plate (30s first layer exposure time versus 16 s exposure time for the rest of the layers), contributing to a crosslinking gradient along the z-axis, as opposed to the bulk crosslinking that occurs during moulding.

The load capability of the tubular conduits was investigated via compression between two plates to elicit radial strength measurements (Mi et al., 2019; Zhou et al., 2019; Emechebe et al., 2020). Upon compression, the 3D-printed conduits showed excellent compression resistance reaching a maximum load of approximately 3N (Fig. 6D). Interestingly, upon load removal, most of the constructs (two out of three) returned to their original shape, thereby indicating that the changes in formulation, especially the use of a low MW PEGDA compared to similar investigations, still resulted in a robust and tough hydrogel. The failure of sample 3 might have originated from structural defects of the tubular wall either during the 3D-printing process or whilst handling the sample post-printing, however confirmation of this requires further investigation, potentially using a greater sample number. However, given the limited number of samples this requires further investigation. Here, an introductory evaluation into the mechanical behaviour of the 3D-printed tubular conduits is presented, but further studies (e.g., fatigue and durability analysis, radial load evaluation in tension, anisotropy evaluation, suture retention strength, burst pressure, and compliance analysis) and the effect of storage and aging, are required to assess the suitability of this material and manufacturing method for the production of aortic graft substitutes. Moreover, given that both the alginate and PEGDA monomers are known for their lack of cell binding moieties, ongoing work is currently investigating the biofunctionalization of this hydrogel formulation to improve cell adhesion, and thus promote endothelialisation. Nonetheless, this work provides a promising step forward for the development of mechanically relevant, patient-specific aortic grafts, particularly through the ability of this fabrication method to be able to also produce complex structures (branching and bifurcations (Fig. 7)) at high precision and rapid fabrication times.

5. Concluding remarks

Synthetic vascular grafts play a crucial role in the treatment of CVD. In particular, Dacron® grafts have proved to be lifesaving in the surgical treatment of aortic aneurysms. However, the recurrence of graft-related complications and their impact on cardiovascular homeostasis raises the question of their long-term suitability both for the patient's health and from an economical perspective. Here, the use of an alginate:PEGDA IPN hydrogel was introduced to potentially replace existing vascular graft materials. Mechanical characterisation of this hydrogel formulation demonstrated some similarity in elastic properties to those reported in the literature for the human aorta. Furthermore, by exploring two different fabrication methods, moulding and SLA 3D-printing, the latter was identified as a suitable manufacturing technique that not only preserves the mechanical properties of the material but also allows the faithful replication of the aorta's anatomy. Overall, albeit preliminary, this approach shows great potential towards the contribution to future fabrication of patient-specific, biomechanically-relevant vascular grafts.

CRediT authorship contribution statement

Lisa Asciak: Writing – review & editing, Writing – original draft, Methodology, Investigation, Formal analysis, Data curation, Conceptualization. **Roger Domingo-Roca:** Writing – review & editing, Resources, Funding acquisition. **Jamie R. Dow:** Writing – review & editing. **Robbie Brodie:** Writing – review & editing, Supervision, Funding acquisition, Conceptualization. **Niall Paterson:** Writing – review & editing, Supervision, Funding acquisition, Conceptualization. **Philip E. Riches:** Resources, Writing - review & editing. **Wenmiao Shu:** Writing – review & editing, Supervision, Funding acquisition, Conceptualization. **Christopher McCormick:** Writing – review & editing, Supervision, Resources, Funding acquisition, Conceptualization.

Declaration of competing interest

The authors declare the following financial interests/personal relationships which may be considered as potential competing interests:

Lisa Asciak reports financial support was provided by Terumo Aortic. Christopher McCormick reports equipment, drugs, or supplies was provided by Terumo Aortic. If there are other authors, they declare that they have no known competing financial interests or personal relationships that could have appeared to influence the work reported in this paper.

Data availability

Data will be made available on request.

Acknowledgements

This work was financially supported by Terumo Aortic Ltd., the Scottish Research Partnership in Engineering National Manufacturing Institute Scotland – Industry Doctorate Programme (SRPe NMIS-IDP/006), and the Fund for the Replacement of Animals in Medical Experiments (FRAME, FIGStrat21). The authors would also like to acknowledge the help and support provided by Mrs. C. Henderson and Mr. S. Murray from the Department of Biomedical Engineering (University of Strathclyde).

Appendix A. Supplementary data

Supplementary data to this article can be found online at https://doi.org/10.1016/j.jmbbm.2024.106531.

References

Amabili, M., Prabakaran, B., Isabella, B., Ivan, D.B., Giovanni, F., Giulio, F., Francesco, G., Chloé, P., 2020. Nonlinear dynamics of human aortas for material characterization. Phys. Rev. 10 (1), 011015. X.

Antunes, M., Bonani, W., Reis, R.L., Migliaresi, C., Ferreira, H., Motta, A., Neves, N.M., 2021. Development of alginate-based hydrogels for blood vessel engineering. Mater. Sci. Eng. C, 112588.

Asciak, L., Gilmour, L., Williams, J.A., Foster, E., Díaz-García, L., McCormick, C., Windmill, J.F.C., Mulvana, H.E., Jackson-Camargo, J.C., Domingo-Roca, R., 2023. Investigating multi-material hydrogel three-dimensional printing for *in vitro*

representation of the neo-vasculature of solid tumours: a comprehensive mechanical analysis and assessment of nitric oxide release from human umbilical vein endothelial cells. R. Soc. Open Sci. 10 (8), 230929.
Benjamin, A.D., Abbasi, R., Owens, M., Olsen, R.J., Walsh, D.J., LeFevre, T.B., Wilking, J. N., 2019. 'Light-based 3D printing of hydrogels with high-resolution channels'. Biomedical Physics & Engineering Express 5 (2), 025035.
Boularaoui, S., Al Hussein, G., Khan, K.A., Christoforou, N., Stefanini, C., 2020. An overview of extrusion-based bioprinting with a focus on induced shear stress and its effect on cell viability. Bioprinting 20, e00093.
Burke, G., Devine, D.M., Major, I., 2020. Effect of stereolithography 3D printing on the properties of PEGDMA hydrogels. Polymers 12 (9), 2015.
Busby, G.A., Grant, M.H., MacKay, S.P., Riches, P.E., 2013. Confined compression of collagen hydrogels. J. Biomech. 46 (4), 837–840.
Bustos, C.A., García-Herrera, C.M., Celentano, D.J., 2016. Mechanical characterisation of Dacron graft: Experiments and numerical simulation. J. Biomech. 49 (1), 13–18.
Callaghan, F.M., Grieve, S.M., 2018. Normal patterns of thoracic aortic wall shear stress measured using four-dimensional flow MRI in a large population. Am. J. Physiol. Heart Circ. Physiol. 315 (5), H1174–H1181.
Camasão, D.B., Mantovani, D., 2021. The mechanical characterization of blood vessels and their substitutes in the continuous quest for physiological-relevant performances. A critical review. Materials Today Bio 10, 100106.
Cattelan, G., Guerrero Gerbolés, A., Foresti, R., Pramstaller, P.P., Rossini, A., Miragoli, M., Caffarra Malvezzi, C., 2020. Alginate formulations: current developments in the race for hydrogel-based cardiac regeneration. Front. Bioeng. Biotechnol. 8.
Chimene, D., Kaunas, R., Gaharwar, A.K., 2020. Hydrogel bioink reinforcement for additive manufacturing: a focused review of emerging strategies. Adv. Mater. 32 (1), 1902026.
Cristovão, A.F., Sousa, D., Silvestre, F., Ropio, I., Gaspar, A., Henriques, C., Velhinho, A., Baptista, A.C., Faustino, M., Ferreira, I., 2019. Customized tracheal design using 3D printing of a polymer hydrogel: influence of UV laser cross-linking on mechanical properties. 3D Printing in Medicine 5 (1), 12.
Domingo-Roca, R., Gilmour, L., Dobre, O., Sarrigianidis, S., Sandison, M.E., O'Leary, R., Jackson-Camargo, J.C., Mulvana, H.E., 2022. 3D printing of noncytotoxic high-resolution microchannels in Bisphenol-a ethoxylate dimethacrylate tissue-mimicking materials. 3D Print. Addit. Manuf. 10, 1101–1109.
Emechebe, G.A., Obiweluozor, F.O., Jeong, I.S., Park, J.-K., Park, C.H., Kim, C.S., 2020. Merging 3D printing with electrospun biodegradable small-caliber vascular grafts immobilized with VEGF. Nanomed. Nanotechnol. Biol. Med. 30, 102306.
Farkas, A.Z., Galatanu, S.-V., Nagib, R., 2023. The influence of printing layer thickness and orientation on the mechanical properties of DLP 3D-printed dental resin. Polymers 15 (5), 1113.
Faturechi, R., Hashemi, A., Abolfathi, N., Solouk, A., 2019. Mechanical guidelines on the properties of human healthy arteries in the design and fabrication of vascular grafts: experimental tests and quasi-linear viscoelastic model. Acta Bioeng. Biomech. 21 (3), 13–21.
Gao, Q., He, Y., Fu, J.-Z., Liu, A., Ma, L., 2015. Coaxial nozzle-assisted 3D bioprinting with built-in microchannels for nutrients delivery. Biomaterials 61, 203–215.
Ghanizadeh Tabriz, A., Hermida, M.A., Leslie, N.R., Shu, W., 2015. Three-dimensional Bioprinting of Complex Cell Laden Alginate Hydrogel Structures.
Ghanizadeh Tabriz, A., Mills, C.G., Mullins, J.J., Davies, J.A., Shu, W., 2017. Rapid Fabrication of Cell-Laden Alginate Hydrogel 3D Structures by Micro Dip-Coating.
Golledge, J., 2019. Abdominal aortic aneurysm: update on pathogenesis and medical treatments. Nat. Rev. Cardiol. 16 (4), 225–242.
González, G., Baruffaldi, D., Martinengo, C., Angelini, A., Chiappone, A., Roppolo, I., Pirri, C.F., Frascella, F., 2020. Materials testing for the development of biocompatible devices through vat-polymerization 3d printing. Nanomaterials 10 (9), 1788.
González-Díaz, E.C., Varghese, S., 2016. Hydrogels as extracellular matrix analogs. Gels 2 (3), 20.
Grigoryan, B., Paulsen, S.J., Corbett, D.C., Sazer, D.W., Fortin, C.L., Zaita, A.J., Greenfield, P.T., Calafat, N.J., Gounley, J.P., Ta, A.H., 2019. Multivascular networks and functional intravascular topologies within biocompatible hydrogels. Science 364 (6439), 458–464.
Growney Kalaf, E.A., Flores, R., Bledsoe, J.G., Sell, S.A., 2016. Characterization of slow-gelling alginate hydrogels for intervertebral disc tissue- engineering applications. Mater. Sci. Eng. C 63, 198–210.
Hisham, M., Saravana Kumar, G., Deshpande, A.P., 2022. Process optimization and optimal tolerancing to improve dimensional accuracy of vat-photopolymerized functionally graded hydrogels. Results in Engineering 14, 100442.
Holland, I., Logan, J., Shi, J., McCormick, C., Liu, D., Shu, W., 2018. 3D biofabrication for tubular tissue engineering. Bio-Design and Manufacturing 1 (2), 89–100.
Hong, S., Sycks, D., Chan, H.F., Lin, S., Lopez, G.P., Guilak, F., Leong, K.W., Zhao, X., 2015. 3D printing of highly stretchable and tough hydrogels into complex, cellularized structures. Adv. Mater. 27 (27), 4035–4040.
Huang, D., Huang, Y., Xiao, Y., Yang, X., Lin, H., Feng, G., Zhu, X., Zhang, X., 2019. Viscoelasticity in natural tissues and engineered scaffolds for tissue reconstruction. Acta Biomater. 97, 74–92.
Ioannou, C.V., Morel, D.R., Katsamouris, A.N., Katranitsa, S., Startchik, I., Kalangos, A., Westerhof, N., Stergiopulos, N., 2009. Left ventricular hypertrophy induced by reduced aortic compliance. J. Vasc. Res. 46 (5), 417–425.
Jejurikar, A., Lawrie, G., Martin, D., Grøndahl, L., 2011. A novel strategy for preparing mechanically robust ionically cross-linked alginate hydrogels. Biomed. Mater. 6 (2), 025010.
Ji, D., Park, J.M., Oh, M.S., Nguyen, T.L., Shin, H., Kim, J.S., Kim, D., Park, H.S., Kim, J., 2022. Superstrong, superstiff, and conductive alginate hydrogels. Nat. Commun. 13 (1), 3019.
Khilnani, B., Leon, K., Pino, C., Drake, S., Shandas, R., Lammers, S.R., 2023. Gravity-assisted 3D bioprinting: using gravity as a design input to build high aspect-ratio structures. Bioprinting 32, e00277.
Krishnamoorthy, S., Zhang, Z., Xu, C., 2019. Biofabrication of three-dimensional cellular structures based on gelatin methacrylate–alginate interpenetrating network hydrogel. J. Biomater. Appl. 33 (8), 1105–1117.
Kuo, C.K., Ma, P.X., 2001. Ionically crosslinked alginate hydrogels as scaffolds for tissue engineering: Part 1. Structure, gelation rate and mechanical properties. Biomaterials 22 (6), 511–521.
Kuo, C.K., Ma, P.X., 2008. Maintaining dimensions and mechanical properties of ionically crosslinked alginate hydrogel scaffolds in vitro. J. Biomed. Mater. Res. 84 (4), 899–907.
Lee, K.Y., Mooney, D.J., 2012. Alginate: properties and biomedical applications. Prog. Polym. Sci. 37 (1), 106–126.
Lejay, A., Geny, B., Kolh, P., Chakfé, N., 2019. Effects of aortic graft implantation on heart and downstream vessels: an artery is not a rigid pipe. Eur. J. Vasc. Endovasc. Surg. 58 (4), 477–478.
Levato, R., Dudaryeva, O., Garciamendez-Mijares, C.E., Kirkpatrick, B.E., Rizzo, R., Schimelman, J., Anseth, K.S., Chen, S., Zenobi-Wong, M., Zhang, Y.S., 2023. Light-based vat-polymerization bioprinting. Nature Reviews Methods Primers 3 (1), 47.
Liu, J., Zheng, H., Poh, P.S.P., Machens, H.-G., Schilling, A.F., 2015. Hydrogels for engineering of perfusable vascular networks. Int. J. Mol. Sci. 16 (7), 15997–16016.
Ma, C., Li, W., Li, D., Chen, M., Wang, M., Jiang, L., Mille, L.S., Garciamendez, C.E., Zhao, Z., Zhou, Q., 2022. Photoacoustic imaging of 3D-printed vascular networks. Biofabrication 14 (2), 025001.
Melchiorri, A.J., Hibino, N., Best, C., Yi, T., Lee, Y., Kraynak, C., Kimerer, L.K., Krieger, A., Kim, P., Breuer, C.K., 2016. 3D-printed biodegradable polymeric vascular grafts. Adv. Healthcare Mater. 5 (3), 319–325.
Mi, H.-Y., Jiang, Y., Jing, X., Enriquez, E., Li, H., Li, Q., Turng, L.-S., 2019. Fabrication of triple-layered vascular grafts composed of silk fibers, polyacrylamide hydrogel, and polyurethane nanofibers with biomimetic mechanical properties. Mater. Sci. Eng. C 98, 241–249.
Michael Lee, J., Wilson G, J., 1986. Anisotropic tensile viscoelastic properties of vascular graft materials tested at low strain rates. Biomaterials 7 (6), 423–431.
Mondschein, R.J., Kanitkar, A., Williams, C.B., Verbridge, S.S., Long, T.E., 2017. Polymer structure-property requirements for stereolithographic 3D printing of soft tissue engineering scaffolds. Biomaterials 140, 170–188.
Mørch, Y.A., Donati, I., Strand, B.L., Skjåk-Braek, G., 2006. Effect of Ca2+, Ba2+, and Sr2+ on alginate microbeads. Biomacromolecules 7 (5), 1471–1480.
Munoz-Pinto, D.J., Jimenez-Vergara, A.C., Gharat, T.P., Hahn, M.S., 2015. Characterization of sequential collagen-poly(ethylene glycol) diacrylate interpenetrating networks and initial assessment of their potential for vascular tissue engineering. Biomaterials 40, 32–42.
Murphy, C.A., Lim, K.S., Woodfield, T.B., 2022. Next evolution in organ-scale biofabrication: bioresin design for rapid high-resolution vat polymerization. Adv. Mater. 34 (20), 2107759.
Ni, R., Qian, B., Liu, C., Liu, X., Qiu, J., 2018. A cross-linking strategy with moderated pre-polymerization of resin for stereolithography. RSC Adv. 8 (52), 29583–29588.
Obrien, T., Morris, L., McGloughlin, T., 2008. Evidence suggests rigid aortic grafts increase systolic blood pressure: results of a preliminary study. Med. Eng. Phys. 30 (1), 109–115.
Parak, A., Pradeep, P., du Toit, L.C., Kumar, P., Choonara, Y.E., Pillay, V., 2019. Functionalizing bioinks for 3D bioprinting applications. Drug Discov. Today 24 (1), 198–205.
Roth, G.A., Mensah, G.A., Johnson, C.O., Addolorato, G., et al., 2020. Global burden of cardiovascular diseases and risk factors, 1990–2019: update from the GBD 2019 study. J. Am. Coll. Cardiol. 76 (25), 2982–3021.
Saini, J., Dowling, L., Kennedy, J., Trimble, D., 2020. 'Investigations of the mechanical properties on different print orientations in SLA 3D printed resin'. Proc. IME C J. Mech. Eng. Sci. 234 (11), 2279–2293.
Seo, H., Heo, S.G., Lee, H., Yoon, H., 2017. Preparation of PEG materials for constructing complex structures by stereolithographic 3D printing. RSC Adv. 7 (46), 28684–28688.
Singh, C., Wong, S.C., Wang, X., 2015. Medical textiles as vascular implants and their success to mimic natural arteries. J. Funct. Biomater. 6 (3).
Spadaccio, C., Nappi, F., Al-Attar, N., Sutherland, F.W., Acar, C., Nenna, A., Trombetta, M., Chello, M., Rainer, A., 2016. Old myths, new concerns: the long-term effects of ascending aorta replacement with Dacron grafts. Not all that glitters is gold. Journal of Cardiovascular Translational Research 9 (4), 334–342.
Sun, J.-Y., Zhao, X., Illeperuma, W.R.K., Chaudhuri, O., Oh, K.H., Mooney, D.J., Vlassak, J.J., Suo, Z., 2012. Highly stretchable and tough hydrogels. Nature 489 (7414), 133–136.
Swerdlow, N.J., Wu, W.W., Schermerhorn, M.L., 2019. Open and endovascular management of aortic aneurysms. Circ. Res. 124 (4), 647–661.
Tai, N.R., Salacinski, H.J., Edwards, A., Hamilton, G., Seifalian, A.M., 2000. Compliance properties of conduits used in vascular reconstruction. BJS (British Journal of Surgery) 87 (11), 1516–1524.
Tan, E. Y. S. and Yeong, W. Y. 'Concentric Bioprinting of Alginate-Based Tubular Constructs Using Multi-Nozzle Extrusion-Based Technique'.
Teng, Z., Feng, J., Zhang, Y., Huang, Y., Sutcliffe, M.P.F., Brown, A.J., Jing, Z., Gillard, J. H., Lu, Q., 2015. Layer- and direction-specific material properties, extreme extensibility and ultimate material strength of human abdominal aorta and aneurysm: a uniaxial extension study. Ann. Biomed. Eng. 43 (11), 2745–2759.

The Biomedical 3D printing community, 2023. Embodi3D. Available at: https://www.embodi3d.com/files/file/55739-abdominal-aorta/. (Accessed 9 August 2022).
Tremblay, D., Zigras, T., Cartier, R., Leduc, L., Butany, J., Mongrain, R., Leask, R.L., 2009. A comparison of mechanical properties of materials used in aortic arch reconstruction. Ann. Thorac. Surg. 88 (5), 1484–1491.
Unkovskiy, A., Bui, P.H.-B., Schille, C., Geis-Gerstorfer, J., Huettig, F., Spintzyk, S., 2018. Objects build orientation, positioning, and curing influence dimensional accuracy and flexural properties of stereolithographically printed resin. Dent. Mater. 34 (12), e324–e333.
Vallabhaneni, S.R., Gilling-Smith, G.L., How, T.V., Carter, S.D., Brennan, J.A., Harris, P. L., 2004. Heterogeneity of tensile strength and matrix metalloproteinase activity in the wall of abdominal aortic aneurysms. J. Endovasc. Ther. 11 (4), 494–502.
Vardoulis, O., Coppens, E., Martin, B., Reymond, P., Tozzi, P., Stergiopulos, N., 2011. Impact of aortic grafts on arterial pressure: a computational fluid dynamics study. Eur. J. Vasc. Endovasc. Surg. 42 (5), 704–710.
Wang, D., Xu, Y., Li, Q., Turng, L.-S., 2020. Artificial small-diameter blood vessels: materials, fabrication, surface modification, mechanical properties, and bioactive functionalities. J. Mater. Chem. B 8 (9), 1801–1822.
Xu, C., Dai, G., Hong, Y., 2019. Recent advances in high-strength and elastic hydrogels for 3D printing in biomedical applications. Acta Biomater. 95, 50–59.
Yang, Y., Zhou, Y., Lin, X., Yang, Q., Yang, G., 2020. Printability of external and internal structures based on digital light processing 3D printing technique. Pharmaceutics 12 (3), 207.
Yu, C., Schimelman, J., Wang, P., Miller, K.L., Ma, X., You, S., Guan, J., Sun, B., Zhu, W., Chen, S., 2020. Photopolymerizable biomaterials and light-based 3D printing strategies for biomedical applications. Chem. Rev. 120 (19), 10695–10743.
Zhang, H., Wang, L., Song, L., Niu, G., Cao, H., Wang, G., Yang, H., Zhu, S., 2011. 'Controllable properties and microstructure of hydrogels based on crosslinked poly (ethylene glycol) diacrylates with different molecular weights'. J. Appl. Polym. Sci. 121 (1), 531–540.
Zhang, M., Qian, T., Deng, Z., Hang, F., 2021. 3D printed double-network alginate hydrogels containing polyphosphate for bioenergetics and bone regeneration. Int. J. Biol. Macromol. 188, 639–648.
Zhijie, W., Mark, J.G., Naomi, C.C., 2016. Viscoelastic properties of cardiovascular tissues. In: Mohamed Fathy, E.-A. (Ed.), Viscoelastic and Viscoplastic Materials. IntechOpen, Rijeka. Ch. 7.
Zhou, Y., Gui, Q., Yu, W., Liao, S., He, Y., Tao, X., Yu, Y., Wang, Y., 2019. Interfacial diffusion printing: an efficient manufacturing technique for artificial tubular grafts. ACS Biomater. Sci. Eng. 5 (11), 6311–6318.
Zia, A.W., Liu, R., Wu, X., 2022. Structural design and mechanical performance of composite vascular grafts. Bio-Design and Manufacturing 5 (4), 757–785.